RF performance comparison of several H plane rectangular waveguide filters loaded with circular dielectric posts

Carmen Bachiller*, *Member, IEEE,* Héctor Esteban**, *Member, IEEE,* Fernando Díaz†, José Vicente Morro††, *Member, IEEE,* Vicente E. Boria⋆, *Senior Member, IEEE*

Departamento de Comunicaciones, Universidad Politécnica de Valencia, 46022 Valencia, Spain

e-mails: *mabacmar@dcom.upv.es; **hesteban@dcom.upv.es; †ferdiaca@teleco.upv.es; ††jomorros@dcom.upv.es; ⋆vboria@dcom.upv.es

Abstract

The paper presents a RF performance comparison between several H plane geometry filters based on rectangular waveguide technology. The basic all metal filter of resonant cavities is compared to filters loaded with circular dielectric resonators, either in propagative or evanescent mode. The use of these resonators is claimed to reduce the length of the filter, increase the rejection band until the first spurious frequency and to improve the voltage magnification factor (VMF), at the cost of increasing the losses. So, in order to properly asses and quantify the possible advantages of these filters, an accurate analysis of six of them has been developed. All the filters have been designed to have the same electrical response, and the length, losses, rejection band, VMF and fabrication cost for all the filters are compared.

Index Terms

Rectangular waveguides, waveguide filters, dielectric loaded waveguides, voltage magnification factor

I. Introduction

All metallic H plane [1] microwave waveguide filters have been widely used commercially for many applications, such as for communication satellite payloads. These filters have very reduced insertion losses within their operating frequency band, and their construction is considerably simple. On the other hand, metallic filters have significant drawbacks, especially when they are designed for satellite and other spatial applications, since their weight and size are very often too high, and due to the lack of atmosphere, the multipactor effect may limit the amount of power that the filters can handle [2].

An alternative to all metallic waveguide filters is the use of circular dielectric resonators [3], [4], [5], [6], [7]. The use of these resonators, either in propagative [8] or in evanescent mode [9], [10] topologies, provides a reduction of around 50% in mass and volume [8], [9], an increase of thermal stability [11], [12], and, if the dielectric rods are all inductive or H plane, an increase of out-of-band rejection and better field distribution (lower voltage magnification factor), because the peaks of electric field within these filters are concentrated inside the dielectric posts, thus producing a smaller level of electromagnetic field, outside the dielectric posts, than in the case of the all metallic filters [13]. Considering that the multipactor effect can only occur outside the posts, since inside the all inductive dielectric posts breakdown processes would require significantly much more power, it follows that these filters need more power for the multipactor discharge to take place. On the other hand, the introduction of dielectric resonators increases the insertion losses when compared to all metallic filters, and the poor thermal conductivity of the dielectric posts could be a more limiting factor than the multipaction threshold.

Until now there have been few publications regarding the RF performance comparison of filters loaded with dielectric resonators and all metallic solutions. In [13] a preliminary study of the multipaction threshold values of three different topologies of filters loaded with circular dielectric rods was presented. In this work a thorough study of the performance of seven topologies of H plane filters is presented. Figure 1 shows the topologies of these filters. The first one is an all metallic coupled cavities filter. Three types of propagative filters loaded with circular dielectric rods have been considered. They differ in whether the dielectric resonator is a single post, two posts or a multilayer post in each cavity. Finally, three types of evanescent mode filters loaded with circular dielectric

resonators have been studied, with either centered, decentered or double posts.

All seven filters have been designed to have the same electrical Chebychev response, and their performance in terms of length, insertion losses, out-of-band rejection, and voltage magnification factor are compared and discussed.

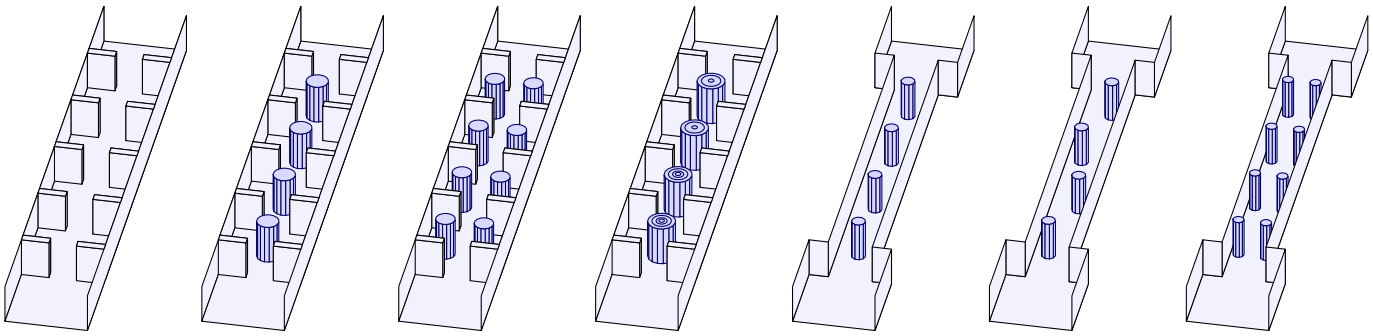

(a) All metallic (b) Single post (c) Double post (d) Multilayer post (e) Evanescent single post (f) Evanescent off-centered post (g) Evanescent double post

Fig. 1. Topologies of H plane filters under analysis

II. Electromagnetic analysis

In order to study the performance of the filters under study, an accurate and efficient full-wave simulation tool must be used. Commercial all purpose simulation tools such as CST or HFSS could be used. However, the simulation tool is invoked repeatedly by the design strategy described in section III in order to find the optimal dimensions of each filter, so that all of them have the same electrical response for a fair comparison among them. Therefore the efficiency of this analysis tool is essential. For that reason a specific simulation tool for H-plane waveguide devices, which is equally accurate but much faster than commercial software for this type of filters, has been used. This simulation tool is able to compute not only the electrical response (i.e. scattering parameters) of the filter. It also provides the field distribution inside the filter in order to estimate its voltage magnification factor, which is needed to estimate the maximum power without multipaction, acording to the field based multipaction model described in [14].

In order to efficiently analyze the filters, the simulation method used in this work segments the filter into simple building blocks, as shown in figure 2 for the case of the propagative filter with centered posts. The circuital

parameters (multimodal generalized scattering matrices) of all segments are computed, and then the global scattering parameters are found by cascading the scattering matrices with the efficient method presented in [15].

In all the types of filters considered, the proposed segmentation gives raise to three types of segments: empty waveguide segments (blocks 1, 3, 5, 7, 9, ... in figure 2), steps (blocks 2, 4, 8, 10, ... in figure 2), and waveguide segments loaded with centered, decentered, double, or multilayer posts (blocks 6 ... in figure 2).

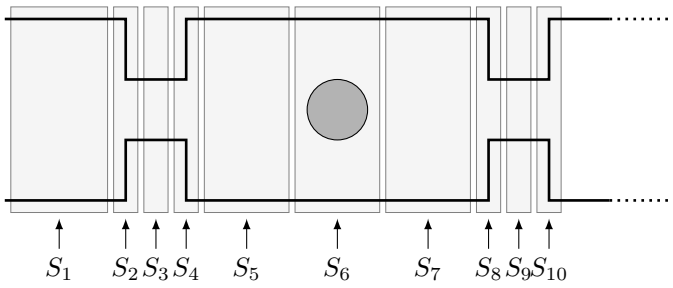

Fig. 2. Segmentation for analysis of the filter of figure 1(b).

The scattering matrices of the empty waveguide segments are computed analytically using standard transmission line theory [16], the scattering matrices of the steps are obtained using the standard mode matching method [17], and the scattering matrices of the waveguide segments loaded with circular posts are calculated with the new efficient method presented in [18].

Once the global scattering matrix, and therefore the reflection and transmission parameters of the whole filter, has been calculated, it is also necessary to obtain the field distribution inside the filter in order to apply the field based multipaction model of [14] and compute the voltage magnification factor. The scattering parameters of all the dielectric posts of the filters of Figure 1 have been obtained with the method described in [18]. The method encloses the dielectric posts in a circumference and expands the field outside as a summation of guided modes of the standard rectangular waveguide, and the field inside as a summation of open space cylindrical modes. These regions are always the same for all the filters of Figure 1. However, for computing the field inside the filter, the specific position of the cylindrical posts has to be considered, and, for each filter, different field regions must be considered, because in each one of these regions the field is reconstructed using the original Mode Matching field expansions (guided and open space cylindrical modes) in a different manner. For conciseness, these field

regions used to reconstruct the field are only presented for the case of the filter of figure 1(b). The different regions used to reconstruct the field in the rest of the filters can be found at [19]. For the filter of figure 1(b), the inner part of the filter is divided into the regions depicted in figure 3 in order to reconstruct the field. The field in all regions, except regions 6b and 6c, can be computed as a summation of the standard guided modes of the empty rectangular waveguide with the appropriate amplitudes. For that purpose, the method proposed in [15] is adequate, since it increases the efficiency for cascading scattering matrices when compared with traditional methods, like the successive connection by pairs [20] or the conversion to ABDC or T matrices [16]. Furthermore, such technique provides with the amplitudes of the progressive and regressive waves in all the accessing ports of all the segments that have been cascaded, once the excitation of the whole filter is defined. These amplitudes allow the calculation of the field in all regions (except 6b and 6c) as summation of standard guided waves of the empty waveguide. In regions 6b and 6c the field is obtained as a summation of the cylindrical open space modes used in the method of [18] to expand the field inside and around the cylindrical posts. This method provides a relation between the amplitudes of the guided and cylindrical modes (see equation (53) in [18]).

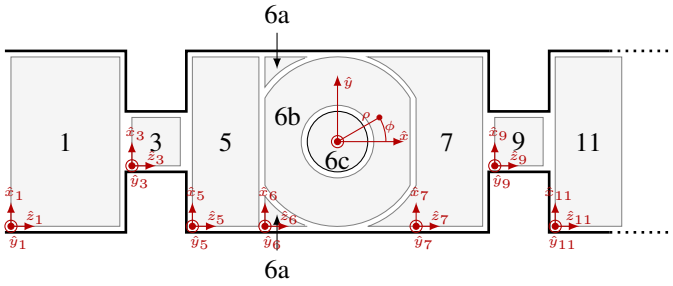

Fig. 3. Different regions for the calculation of the electric field inside the filter of figure 1(b).

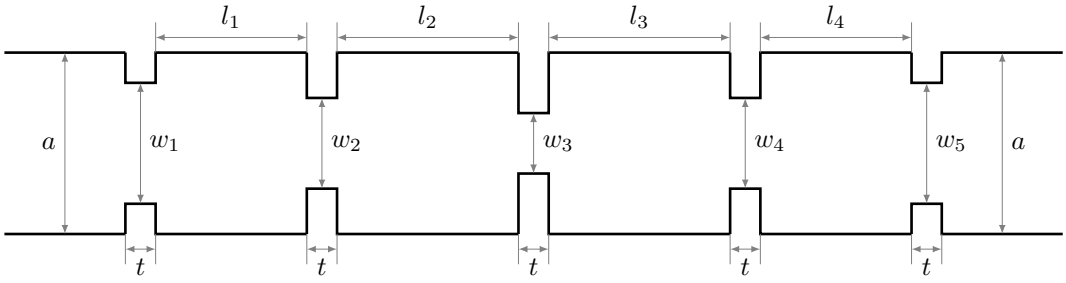

(a) All metallic filter. $a = 19.05$ mm, $t = 2$ mm, $w_1 = w_5 = 10.52$ mm, $w_2 = w_4 = 7.098$ mm, $w_3 = 6.52$ mm, $l_1 = l_4 = 15.68$ mm, $l_2 = l_3 = 17.605$ mm

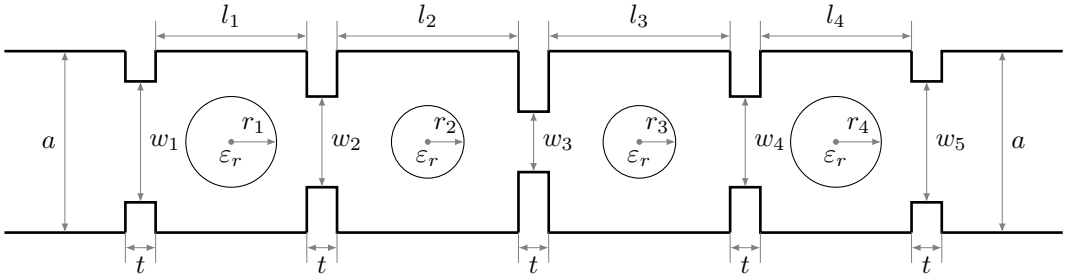

(b) Filter loaded with single circular dielectric posts. $a = 19.05$ mm, $t = 2$ mm, $w_1 = w_5 = 10.37$ mm, $w_2 = w_4 = 6.286$ mm, $w_3 = 6.1$ mm, $l_1 = l_4 = 6.98$ mm, $l_2 = l_3 = 8.28$ mm, $r_1 = r_4 = 2.111$ mm, $r_2 = r_3 = 2.172$ mm, $\varepsilon_r = 24$

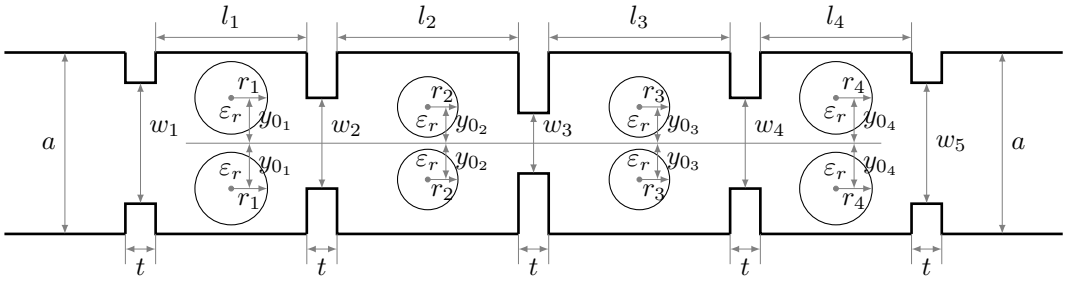

(c) Filter loaded with double circular dielectric posts. $a = 19.05$ mm, $t = 2$ mm, $w_1 = w_5 = 13.37$ mm, $w_2 = w_4 = 6.286$ mm, $w_3 = 6.1$ mm, $l_1 = l_4 = 6.1953$ mm, $l_2 = l_3 = 5.0441$ mm, $r_1 = r_4 = 1.9864$, $r_2 = r_3 = 2.186$ mm, $\varepsilon_r = 24$, $y_{01} = y_{04} = 2.1$ mm, $y_{02} = y_{03} = 3.8072$ mm

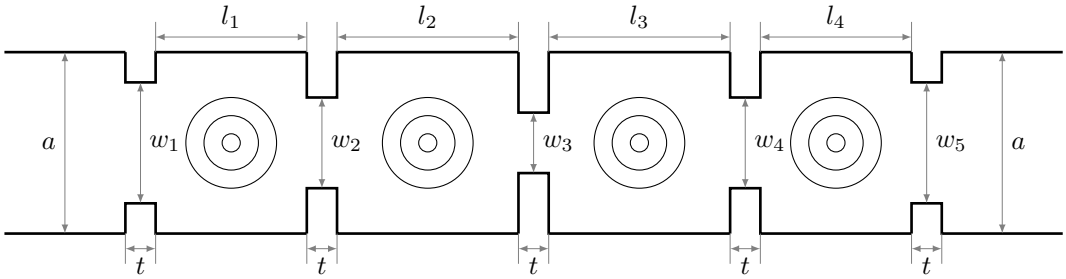

(d) Filter loaded with multilayer circular dielectric posts. $a = 19.05$ mm, $t = 2$ mm, $w_1 = w_5 = 12.8496$ mm, $w_2 = w_4 = 6.6288$ mm, $w_3 = 6.0324$ mm, $l_1 = l_4 = 8.092$ mm, $l_2 = l_3 = 8.7731$ mm, $r_1 = r_4 = (2.2095, 1.2961, 0.6203)$, $r_2 = r_3 = (2.2998, 1.1319, 0.3405)$, $\varepsilon_{r_i} = (21, 24, 27)$, $i \in 1, \ldots, 4$

Fig. 4. Layout and designed parameters of propagative filters.

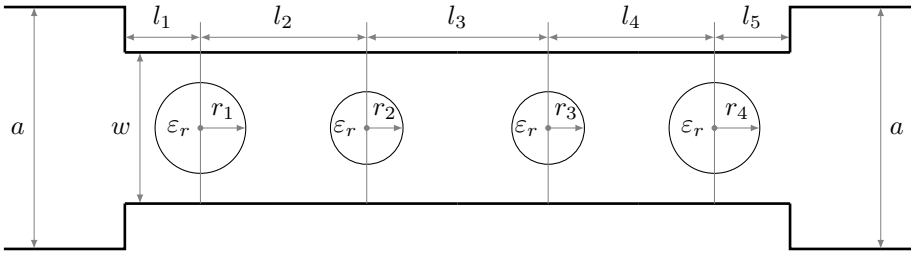

(a) Evanescent mode filter loaded with single circular dielectric posts. $a = 19.05$ mm, $w = 8$ mm, $l_1 = l_5 = 2.4179$ mm, $l_2 = l_4 = 10.182$ mm, $l_3 = 10.9919$ mm, $r_1 = r_4 = 0.777$ mm, $r_2 = r_3 = 2.169$ mm, $\varepsilon_r = 24$

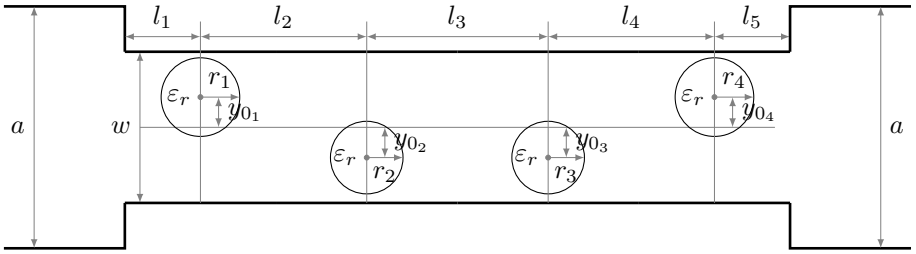

(b) Evanescent mode filter loaded with off-centered circular dielectric posts. $a = 19.05$ mm, $w = 9,5$ mm, $l_1 = l_5 = 3.6938$ mm, $l_2 = l_4 = 11.5609$ mm, $l_3 = 11.6178$ mm, $r_1 = r_4 = 0.732$ mm, $r_2 = r_3 = 1.0933$ mm, $y_{01} = y_{04} = 1.2127$ mm, $y_{02} = y_{03} = 3.4044$ mm, $\varepsilon_r = 24$

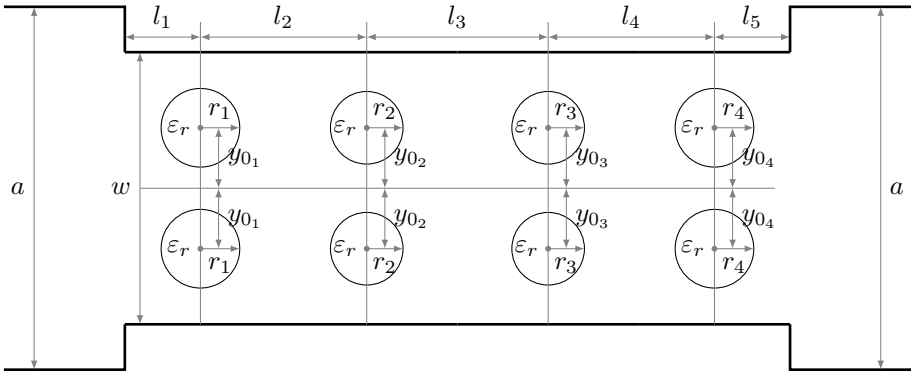

(c) Evanescent mode filter loaded with double circular dielectric posts. $a = 19.05$ mm, $w = 10.686$ mm, $l_1 = l_5 = 4.2457$ mm, $l_2 = l_4 = 13.3238$ mm, $l_3 = 14.784$ mm, $r_1 = r_4 = 1.0305$ mm, $r_2 = r_3 = 1.0433$ mm, $y_{0i} = 4.22$ mm, $i \in 1, \ldots, 4$, $\varepsilon_r = 24$

Fig. 5. Layout and designed parameters of evanescent mode filters.

III. Filter designs

In order to undertake a fair comparison among the seven filter topologies of figure 1, their geometrical parameters have been designed so that they all present the same electrical response. This electrical response has been chosen to be a four pole Chebychev filter centered at 11 GHz with a bandwidth of 300 MHz, which is a typical frequency band for satellite communications. The dielectric posts have been chosen to be of ceramic material with an electric permittivity of $\varepsilon_r = 24$. In the case of multilayer posts, a three layer post has been considered with $\varepsilon_r = 21$ in the inner layer, $\varepsilon_r = 24$ in the middle layer, and $\varepsilon_r = 27$ in the outer layer. The length of all the coupling irises for propagative filters (t in figure 4) has been chosen to be 2 mm.

The first filter (all metallic coupled cavities filter, figure 1(a)), has been designed using the space mapping technique with segmentation and hybrid optimization algorithms, described in [21]. The dimensions of the designed filter are shown in the caption of figure 4(a).

The propagative filters with circular dielectric posts (figures 1(b), 1(c) and 1(d)) have been designed using the strategy presented in [22]. This strategy uses space mapping with segmentation and hybridization of optimization techniques, as well as two optimization levels with two different coarse simulators since in this case it is difficult to obtain a good starting point, as it is possible with all metal filters. The designed filters ans their dimensions are shown in figures 4(b), 4(c) and 4(c).

Finally, the evanescent mode filters with circular dielectric posts (figures 1(e), 1(f) and 1(g)) have been designed using the strategy of [9]. As for propagative filters, a good starting point is difficult to obtain, and a design strategy hybridazing the genetic algorithm and the Nelder Mead simplex method without segmentation of the structure is used to converge to the solution. The dimensions of these three evanescent mode filters are shown in the captions of figures 5(a), 5(b) and 5(c).

Figure 7 depicts the reflection coefficient of the seven designed filters. This result has been obtained segmenting the structure into empty lines, steps, and dielectric loaded waveguides, as explained in section II. Scattering matrices of the empty lines are obtained analytically [16]. Scattering matrices of the steps are obtained using standard Mode Matching [17]. And scattering matrices of the dielectric loaded waveguides are obtained using the method of

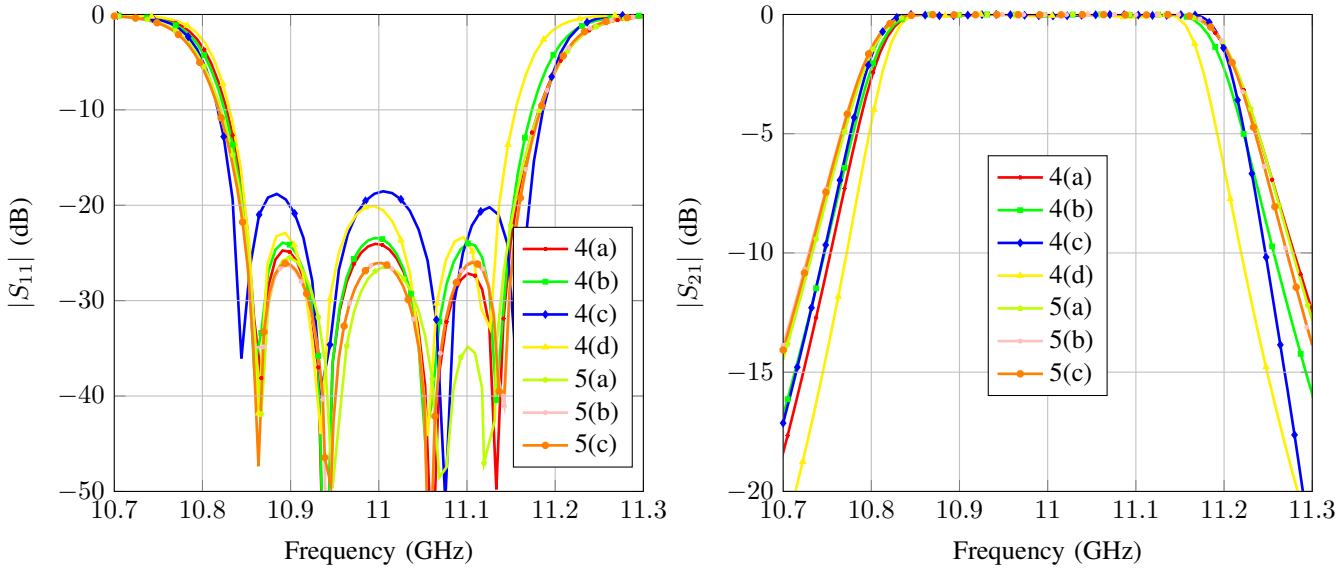

(a) Reflection

(b) Transmission

Fig. 6. Reflection and transmission of the seven designed filters (Figures 4 and 5).

[18]. Then all the scattering matrices are cascaded using the method of [15]. No losses in conductor or dielectric posts have been considered. It can be observed that all of them present a very similar electrical response, so their performance in terms of length, insertion losses, out-of-band rejection, cost and voltage magnification factor can be now fairly compared.

IV. Results

Once all the filters have been designed to have the same electrical response, the following calculations have been performed for each one of them:

- Total physical length of the four pole filter.
- Insertion losses in the pass band assuming a conductivity of $\sigma = 5,96 \cdot 10^7$ S/m for the conductor and a loss tangent of $\tan\delta = 10^{-3}$ for the dielectric posts.
- Out-of-band electrical response in order to estimate the out-of-band rejection of the filter.
- Electric field distribution inside the filter for all the frequencies in the pass band, in order to find the voltage magnification factor.

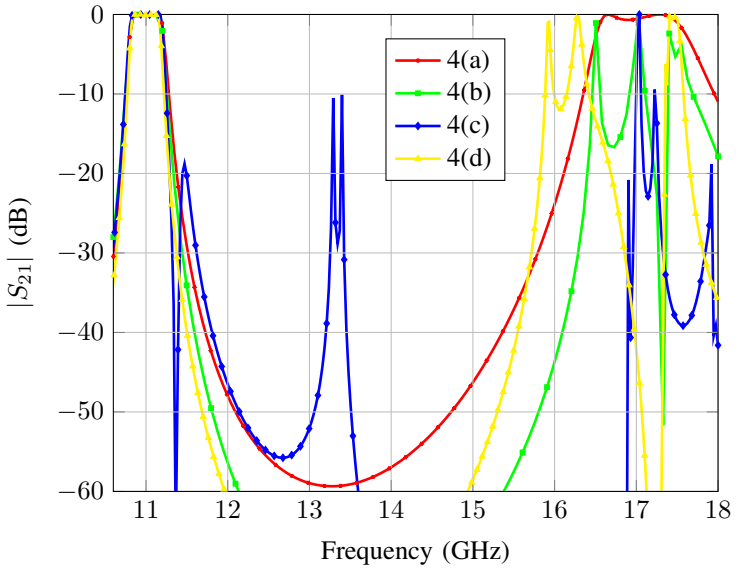

(a) Propagative mode filters

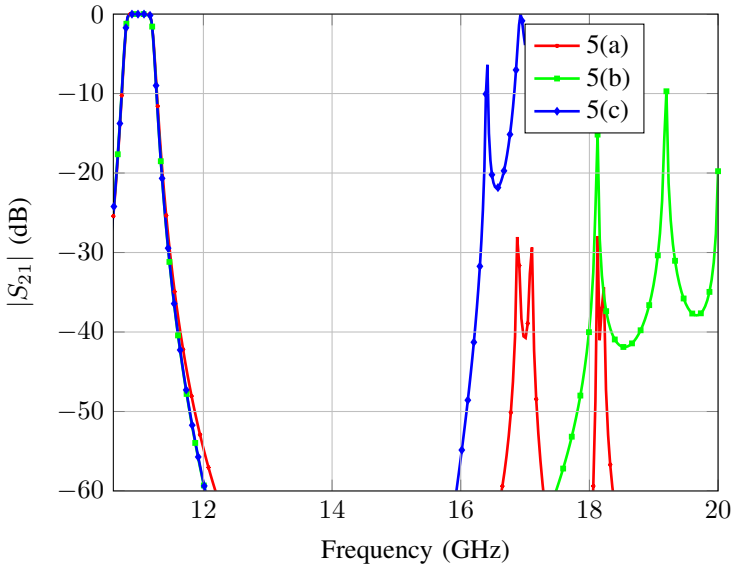

(b) Evanescent mode filters

Fig. 7. Wideband transmission of the seven designed filters (Figures 4 and 5).

- Estimated fabrication cost.

The intermediate results used for estimating the insertion losses, out-of-band rejection, and voltage magnification factor of the propagative filter with centered dielectric posts is presented in this section. Similar intermediate results have been obtained for the other six filters, but they are not included for conciseness. Finally, the performance of the seven filters is compared and discussed in section V.

Figure 8(a) shows the transmission parameter of the propagative filter with centered dielectric resonators in the passband for different values of the dielectric loss tangent. It can be observed that for $\tan\delta = 10^{-3}$, which is a typical value for ceramic dielectric bodies, the insertion loss is around 0,66 dB.

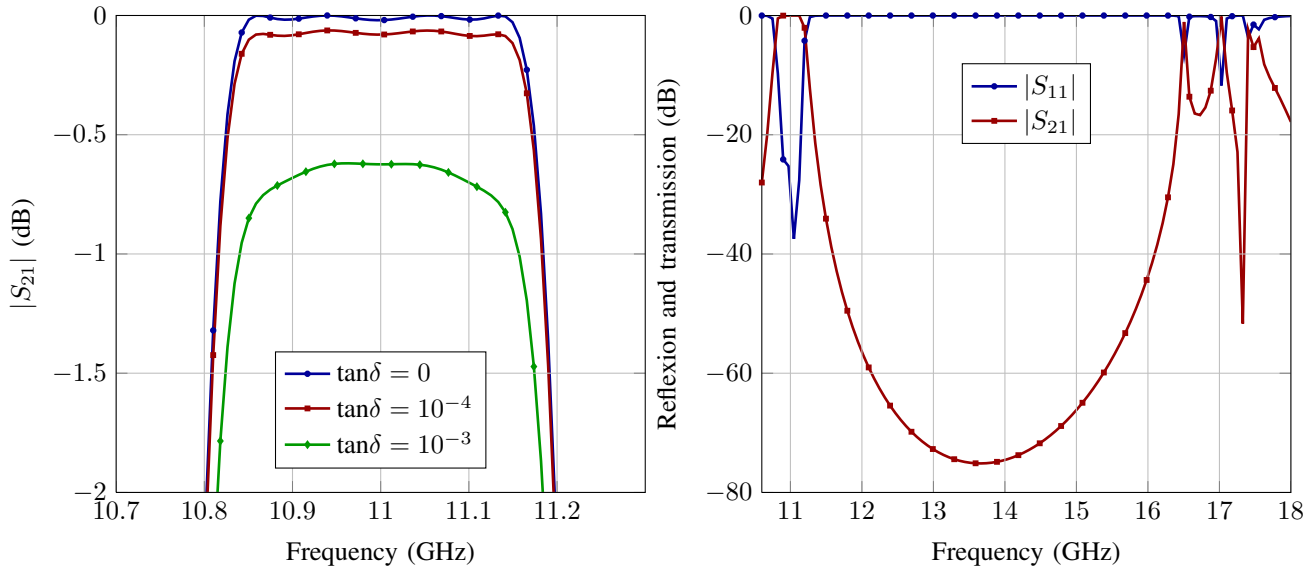

(a) Transmission for different values of the dielectric loss tangent

(b) Out-of-band response

Fig. 8. Results for the filter of figure 4(b)

The out-of-band rejection of this filter has been investigated simulating its electrical response up to 18 GHz (see figure 8(b)). It can be observed that the out-of-band transmission parameter is lower than -20 dB between 11,33 and 16,38 GHz. Therefore the rejected band extends for 5,05 GHz (no losses have been considered for this calculation).

The next feature of the filter that is investigated is the voltage magnification factor. This is estimated using the field based multipaction model of [14]. According to that method, the input power P_{in} can be obtained as

$$P_{in} = \frac{V_{in}^2}{2Z_0} \tag{1}$$

where Z_0 is the characteristic impedance for the fundamental mode TE_{10} in the rectangular waveguide

$$Z_0 = \eta_0 \frac{2b}{a} \frac{\lambda_g}{\lambda} \tag{2}$$

where a and b are the width and height of the rectangular waveguide, λ is the wavelength in free space, λ_g the wavelength inside the guide, and η_0 the impedance of free space.

The voltage at the input of the filter V_{in} is related to the maximum voltage inside the filter by means of a Voltage Magnification Factor (VMF)

$$VMF = \max_{\forall di} \frac{V_{di}}{V_{in}} \tag{3}$$

To prevent multipactor breakdown, the maximum voltage inside the filter must not exceed certain threshold voltage V_{th}. At the limit,

$$\max_{\forall di} V_{di} = V_{th} \tag{4}$$

V_{th} is obtained from the susceptibility curves for different materials and frequencies. Those curves are available with the multipactor calculator of the European Space Agency [23].

Substituting (4) in (3) gives

$$V_{in} = \frac{V_{th}}{VMF} \tag{5}$$

And finally the maximum input power without multipactor breakdown can be obtained substituting (5) in (1),

$$P_{in} = \frac{V_{th}^2}{2\, Z_0 \cdot VMF^2} \tag{6}$$

The minimum value of P_{in} in (6) in the pass band provides the maximum power the the device can handle without risk of multipactor breakdown. From this equation it can be deduced that for the same material and the same characteristic impedance, a smaller VMF (energy better distributed spatially) allows a greater input power without risk of multipaction [24], [13]. However, it must be noted that the dielectric posts are poor thermally conducting materials, so that the power handling capability of the filter can be limited by this factor rather than by the multipaction effect.

For the case of the filter of figure 4(b), the field distribution inside the filter is shown in figure 9(a) for the central frequency of the pass band (f=11 GHz). It can be observed that the maximum fields are always located along the center of the filter. So this is the only place where the field is going to be considered in order to compute the voltage magnification factor.

Figure 9(b) shows the same field distribution of figure 9(a) but just for the central line of the filter. It can be noticed that the maximum field along that line lays inside the dielectric posts. Since the field inside the posts does

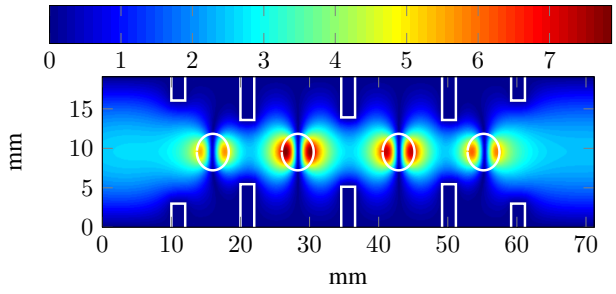

(a) Whole filter. f=11GHz

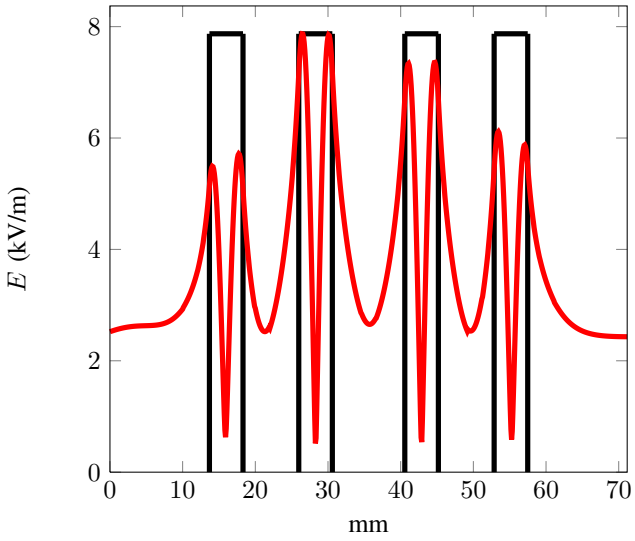

(b) Along central line. f=11GHz

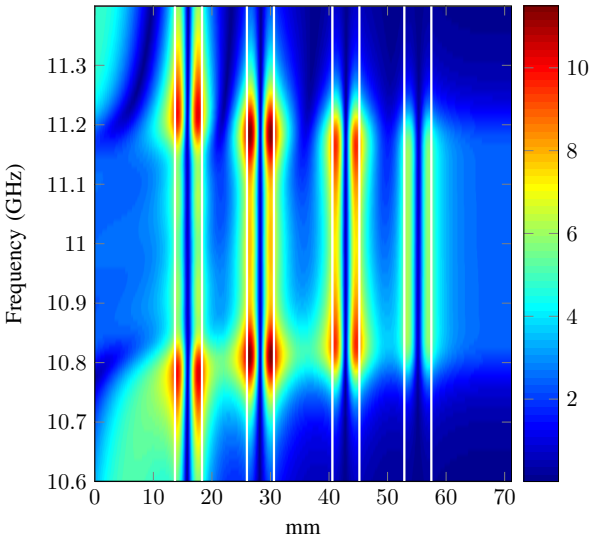

(c) Along central line for different frequencies

Fig. 9. Amplitude of electric field (kV/m) inside the filter of figure 4(b) ($\tan\delta = 0$).

not limit the input power without risk of multipaction, it has not been taken into account for the computation of the VMF.

In order to asses the voltage magnification factor for all the frequencies in the pass band, the field distribution is computed along the central line of the filter for all those frequencies. The result is depicted in figure 9(c). Since the field distribution changes with the frequency, it can be observed that the position inside the filter where the maximum voltage occurs also changes with the frequency.

Using the data from Figure 9(c) the VMF inside the filter can be computed for all the frequencies. The field that lays inside the posts has been discarded. The resulting VMF is shown in Figure IV for different values of the loss tangent inside the dielectric posts. It can be observed that the VMF decreases when the losses increase.

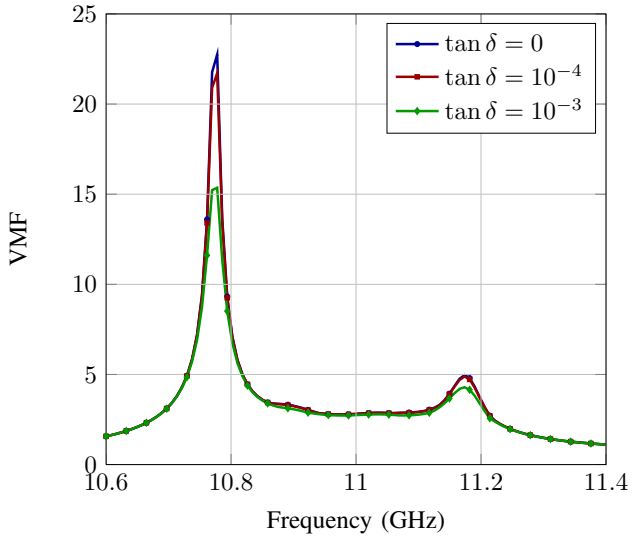

Fig. 10. VMF for the coupled filter with dielectric resonators for $\tan\delta = 0$, $\tan\delta = 10^{-3}$, and $\tan\delta = 10^{-4}$.

Similar calculations as the ones shown here for the coupled filter with dielectric resonators have been done for the other type of filters of Figure 1, where all of them have been designed to present the same electrical response.

Two of the seven types of filters presented here have been manufactured. Specifically, the all metallic filter of Figure 4(a) and the propagative filter with single dielectric posts of Figure 4(b) have been manufactured. The manufactured filters were already presented in [25].

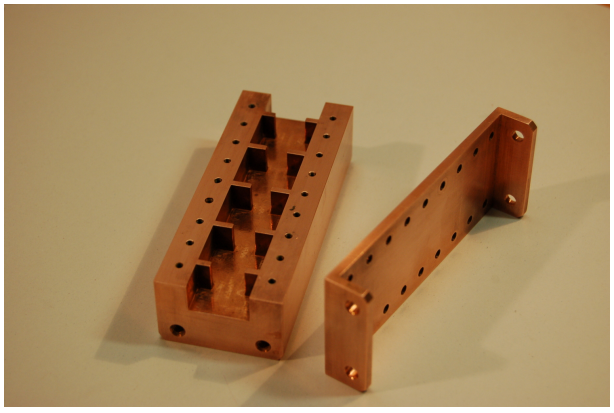

Fig. 11. Manufactured prototype of the filter of Figure 4(a)

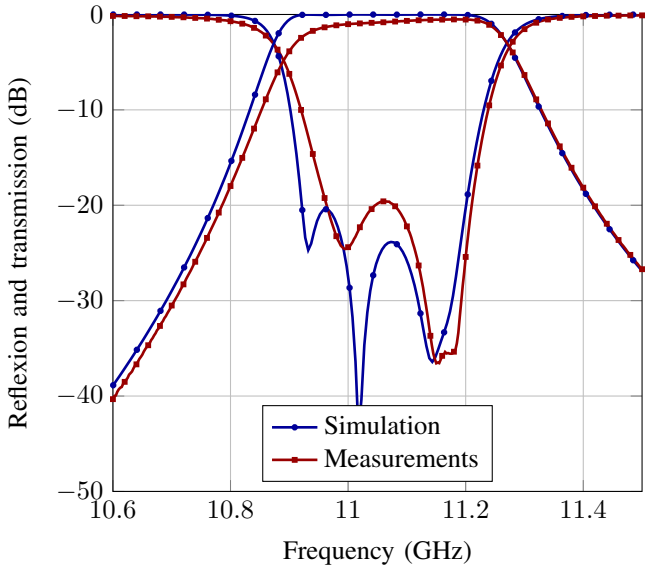

Fig. 12. Comparison of simulation and measurements of the prototype of the filter of Figure 4(a)

Figure 11 shows the manufactured prototype of the all metallic filter of Figure 4(a). This filter was manufactured in copper by Pinach manufacturing company [26]. The filter was manufactured with milling in two pieces, the main body with the coupling irises, and the top wall, as it can be seen in the figure. The total cost for this filter was 900€.

As explained in [25], a dimensional analysis was performed to the prototype in order to measure the real manufactured dimensions, which slightly differed from the designed dimensions due to fabrication tolerances. Figure 12 compares the measured reflection and transmission coefficients with the results from the simulation with the real dimensions provided by the dimensional analysis. As it can be seen, there is a good agreement between simulation and measurements. Better results could be obtained manufacturing with smaller tolerances.

The propagative filter with single centered dielectric posts of Figure 4(b) has also been manufactured. The manufactured prototype is shown in Figure 13. The manufacturing procedure for the filters with dielectric posts is the same as for the all metallic filters, only that the dielectric posts must be properly placed. For that purpose, a circular basement is milled at the bottom wall of the metallic structure of the guide for each dielectric post. Then the dielectric posts are fixed to the basement with epoxi glue and the top wall of the filter is placed and screwed

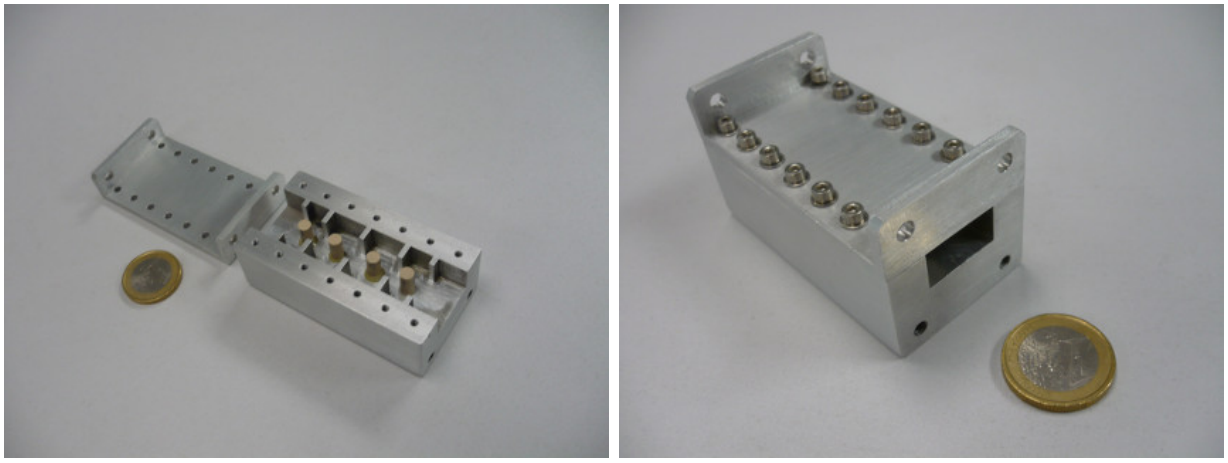

(a) Open without top wall

(b) Closed with top wall screwed

Fig. 13. Manufactured prototype of the filter of Figure 4(b)

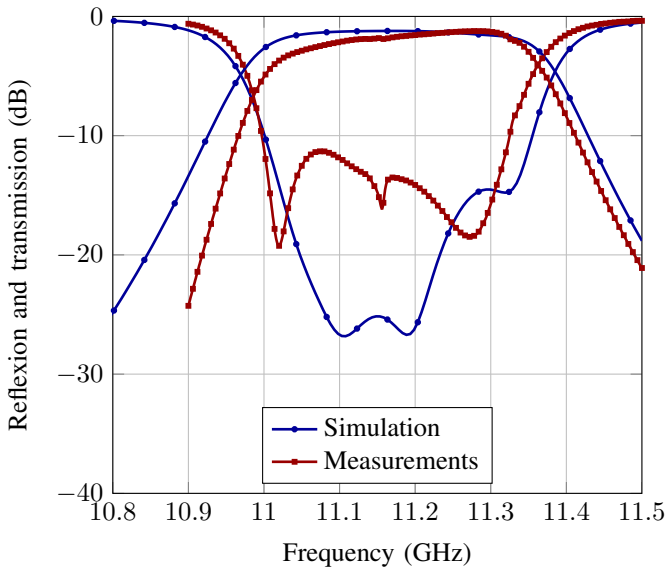

Fig. 14. Comparison of simulation and measurements of the prototype of the filter of Figure 4(b)

to the main body (see Figure 13). The metallic body of this filter was also manufactured by Pinach manufacturing company [26], but this time in aluminium. The manufacturing cost was the same, 900€. The dielectric posts have been bought to Morgan Advanced Materials [27], at the price of 50€ each post. The posts are made of the D20 material (see the technical characteristics of this material in the online catalogue of the manufacturer [27]). According to the data provided by Morgan, the thermal conductivity of this material is 7 W/mK, much lower than,

for example, in the case of aluminium (204 W/mK) or copper (353 W/mK). This low thermal conductivity, together with the increased value of losses, suggest a worse behaviour from thermal point of view than in the case of an all-metallic filter. However, the material D20 is, according to Morgan, stabilized in the range of temperature from $-30°$ to $+85°$, with a temperature coefficient of 0 ppm/°C, so it should be suitable for use in space communications systems. The total cost for this filter, therefore, is $900 + 4 \cdot 50 = 1,100$ €.

Figure 14 compares simulation and measurements for this filter. Besides a dimensional analysis, in this case an accurate estimation of the real value of the permittivity of the dielectric posts at the operating frequency has also been performed, as explained in [25]. Again simulations and measurements are in good agreement.

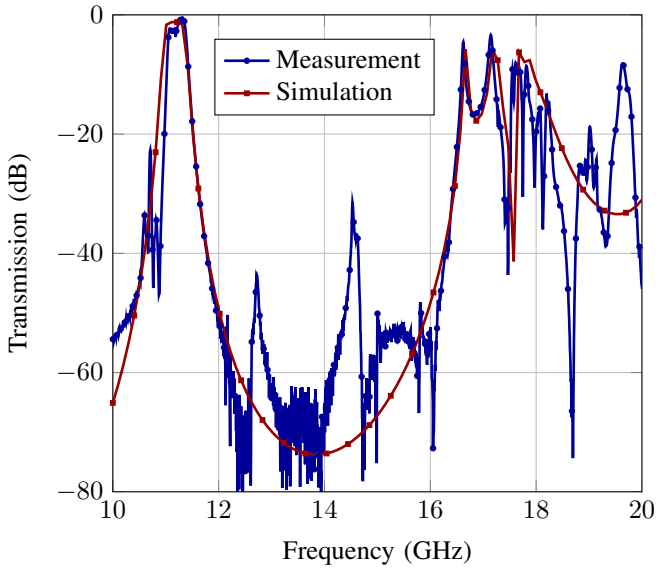

Fig. 15. Wideband measured and simulated response of the prototype of the filter of Figure 4(b)

Figure 15 shows the measured transmission parameter of the prototype of the filter of Figure 4(b) for a wide frequency band, so that the second transmission band can be observed and the out-of-band rejection can be evaluated. The measured frequency response is degraded around 10.5 GHz. This is a consequence of the calibration procedure. Since it is a wideband measurement, the guided TRL standards have not been used (they can only be used with monomode propagation), and only a coaxial calibration has been done. Therefore the coaxial to waveguide transitions have not been deembeded from the measurements. There is a good agreement in the second transmission band

between simulation and measurements.

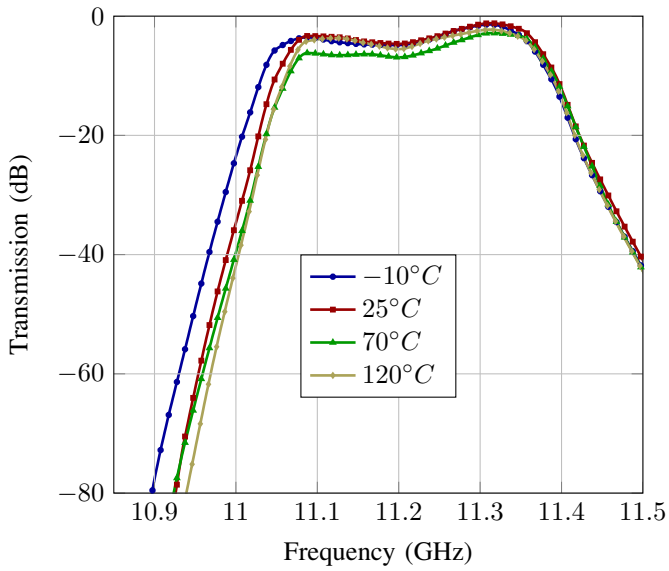

Fig. 16. Variation of the measured transmission parameter of the prototype of the filter of Figure 4(b) with the temperature

As already mentioned, a potential application of this filters could be to realize satellite payload filters. A challenge for satellite payload filters is the operating temperature range, so that the assembly process of the dielectrics into the metallic waveguide is critical since it has to withstand different material thermal expansion coefficient and thermal conductivity. In order to test the behaviour of the prototype of the filter of Figure 4(b) with temperature, measurements over temperature have been performed. The TRL calibration procedure for continuous calibration over temperature in a climatic chamber presented in [28] has been used. The results are shown in Figure 16. As it can be observed, the central frequency and the bandwidth are slightly changed when temperature changes, as it was expected. But these deviations are very similar than for an all metallic filter. Besides, no physical or mechanical degradations in the filter have appeared after the whole temperature cycle.

The other 5 types of filters have not been manufactured, but their cost can be easily estimated. If the filter is evanescent, the filter is smaller, simpler, and requires less material and less time to be manufactured. Therefore, the cost of the metallic shell for the evanescent filter is reduced to 630€. To that price the cost of the dielectric posts (50€ each post) has to be added. The only filter without an estimated cost is the filter with multilayer posts,

since these multilayer posts are not commercially available.

Filter type	Length	Insertion losses	Margin to spurious band	Estimated cost	VMF
Filter of Figure 4(a)	96,5700 mm	0,0106 dB	4,72 GHz	900 €	3.99
Filter of Figure 4(b)	60,5200 mm	0,6606 dB	5,05 GHz	1,100 €	3.02
Filter of Figure 4(c)	52,4788 mm	0,6896 dB	2,08 GHz	1,300 €	2.42
Filter of Figure 4(d)	75,8872 mm	0,7488 dB	5,33 GHz	-	3.06
Filter of Figure 5(a)	56,1917 mm	0,6070 dB	11,34 GHz	830 €	3.76
Filter of Figure 5(b)	62,1272 mm	0,5255 dB	6,74 GHz	830 €	3.67
Filter of Figure 5(c)	69,923 mm	0,4880 dB	5,36 GHz	1,030 €	3.03

TABLE I

PERFORMANCE COMPARISON OF FILTER TYPES.

V. PERFORMANCE COMPARISON OF FILTER TYPES

All the calculus presented in section IV for the filter of Figure 4(b) have also been done for the rest of the filters of Figure 1, in order to be able to compare the performance of all these types of filters, all presenting the same electrical response (central frequency 11 GHz, 300 MHz bandwidth, 20 dB return losses, and dielectric posts with ϵ_r=24 and $\tan\delta = 10^{-3}$). The result of this performance comparison is shown in table I. The value of VMF in the table corresponds to the frequency in the passband where the output power without risk of multipaction is lower, that is, the worst case. The total length provided in the table for the filters includes the input and output empty line sections, and the margin to the first spurious passband is the frequency range outside the main passband where the transmission parameter is below -20 dB.

When comparing the filters of Figure 4(b) and Figure 4(a), that is, the filter with single post and the all-metallic filter, it can be observed that for a single post the posts are located in the path of the main flow of power for the fundamental TE_{10} mode (that is, in the middle of the cavity). This concentrates the majority of the field inside the posts, where the wavelength is smaller, and there is no possibility of multipactor breakdown due to high power levels. Therefore the length of the filter is reduced and the VMF is decreased when compared with the all-metallic filter. But, as the field passes through the lossy resonators, the overall losses are increased. The margin to the spurious band is almost unchanged. So this filter could be a very good alternative to traditional all-metallic filters for those cases where a size reduction and/or a lower VMF is needed, at the expense of higher insertion losses and higher fabrication cost due to the cost of the dielectric posts.

If two posts are placed in the cavities, instead of a single post (see filter of Figure 4(b)), the posts are no longer placed where the maximum flow of power of the fundamental mode takes place. However, the posts attract some field, so the field is more evenly distributed throughout the resonant cavity. So the VMF is lower, since the power is not so much concentrated in just one point as before. The volume of dielectric is larger than with one post, so the losses are slightly increased, the length is reduced, the cost is increased since more posts are needed, and the margin to the spurious band has been largely reduced, probably due to the fact that the two posts favour the propagation of the higher order mode TE_{20}.

The performance of filter of Figure 4(d), the filter with multilayer resonators, is not satisfactory. It achieves a lower length reduction than the other loaded filters when compared with the all-metallic filter. Besides, it is not the best choice for minimizing the VMF, or the margin to the first spurious band. Is is also a structure difficult to manufacture. No estimated cost is provided since we have not found any company that offers commercial multilayer posts. So this structure is not of a great practical interest.

The remaining three filters (Figures 5(a), 5(b), and 5(c)) are evanescent mode filters. The main advantage of these filters is the increase of the out-of-band rejection, that is, the margin to the spurious band, as well as the manufacturing cost reduction. The evanescent mode filter with one centred post (Figure 5(a)), achieves an impressive value of more than 11 GHz to the spurious band. These filters present low losses and good size reduction, similar to those of the propagative filters. So it is a good alternative to the propagative filters if a great out-of-band rejection or

lower manufacturing cost is needed, at the cost of increasing the VMF (this is because there is a great concentration of field outside the posts, where the multipactor discharge can take place).

If the posts of the evanescent mode are off-centred (see Figure 5(b)), the posts are taken away from the main flow of power, and therefore there is less power passing through the posts. This results in a decrease of the losses, an increase of the filter length, and a decrease of the VMF, because the field is more evenly distributed. But, at the same time, there is a reduction of the margin to the spurious band, since the propagation of higher order modes is favoured. The cost is the same as with centred posts.

The evanescent mode filter with double posts (see Figure 5(c)), goes further in the direction of the off-centred post. So it further decreases losses, increases length, decreases VMF, and decreases the margin to the spurious band. It is more expensive than the evanescent filters with single posts.

It can be concluded, therefore, that the election of a particular type of filter depends on the specifications, except the filter with multilayer resonators, whose performance is not interesting. If the losses are the most critical parameter, the traditional all-metallic filter should be chosen. But, if size reduction, voltage magnification factor, or the margin to the spurious band needs to be improved, and a decrease of the losses and an increase of the manufacturing cost can be afforded, the filters of Figures 4(b), 4(c), 5(a), 5(b) and 5(c) are a good alternative. The particular choice of one of these filters depends on the particular need for size reduction, VMF, cost, losses, and margin to the spurious band.

VI. Conclusions

In this work the performance of an all metallic filter has been compared with six different types of filters with dielectric resonators, all in H plane geometry. The results show that the presence of the dielectric posts in all cases increases the losses and reduces the filter length. The rest of the parameters studied (out-of-band rejection, VMF and manufacturing cost) strongly depend on the specific topology. The performance of some topologies are promising, with great advantages when compared with the traditional all metallic filter, but with the only drawback of a greater level of losses. For those applications where the losses and cost are not the limiting factor, these new topologies can be a very interesting alternative, providing much better performance (now accurately quantified) in

terms of length, out-of-band rejection, and VMF.

VII. Acknowledgment

Our acknowledgement to Val Space Consortium for its contribution - Laboratories co-funded by the European Regional Development Fund - A way of making Europe

References

[1] G. L. Matthaei, L. Young, and E. M. T. Jones, *Microwave Filters, Impedance-Matching Networks, and Coupling Structures*. McGraw-Hill, 1964.

[2] R. Udiljak, "Multipactor in low pressure gas and in nonuniform RF field structures," Ph.D. dissertation, Chalmers University of Technology, Goteborg, Sweden, 2007.

[3] J. K. Plourde and C. Ren, "Applications of dielectric resonators in microwave components," *IEEE Trans. Microwave Theory Tech.*, vol. 29, pp. 754–770, August 1981.

[4] R. Lech and J. Mazur, "Propagation in rectangular waveguides periodically loaded with cylindrical posts," *IEEE Microwave and Wireless Components Lett.*, vol. 14, no. 4, pp. 177–179, April 2004.

[5] S. B. Cohn, "Microwave bandpass filters containing high-q dielectric resonators," *IEEE Trans. on Microwave, Theory and Tech.*, 1968.

[6] C. Wang and K. Zaki, "Dielectric resonators and filters," *IEEE Microwave Magazine*, 2007.

[7] S. Fiedziuszko, I. Hunter, T. Itoh, Y. Kobayashi, T. Nishikawa, S. Stitzer, and K. Wakino, "Dielectric materials, devices, and circuits," *IEEE Transactions on Microwave Theory and Techniques*, 2002.

[8] J. V. Morro, H. Esteban, C. Bachiller, and V. E. Boria, "Automated design of complex waveguide filters for space systems: A case study," *Int. J. of RF and Microwave Computer-Aided Engineering*, vol. 17, no. 1, pp. 84–89, January 2007.

[9] C. Bachiller, H. Esteban, V. E. Boria, J. V. Morro, M. Taroncher, and B.Gimeno, "CAD of evanescent mode waveguide filters with circular dielectric resonators," in *Proc. of the 2006 AP-S Int. Symp., pp. 597-600*, Alburquerque, June 2006, pp. 1567–1570.

[10] P. Jarry and J. Beneat, *Advanced Design Techniques and Realizations of Microwave and RF Filters*. Wiley-IEEE Press, 2008.

[11] P. Arcioni, V. E. Boria, M. Bozzi, G. Conciauro, and B. Gimeno, "Analysis of H-plane waveguide components with dielectric obstacles by the BI-RME method," in *Proc. of the 32nd Eu. Microwave Conf.*, Milano, 2002, pp. 1–3.

[12] H. Chung-I and H. A. Auda, "Multiple dielectric posts in a rectangular waveguide," *IEEE Transactions on Microwave Theory and Techniques*, vol. 34, no. 8, pp. 883–891, August 1986.

[13] C. Bachiller, H. Esteban, F. Diaz, V. Boria, and J. Morro, "Comparative study of multipactor breakdown in waveguide H-plane filters loaded with dielectric resonators," in *6th Int. Workshop on Multipactor, Corona and Passive Intermodulation in Space RF hardware*, ESA-ESTEC. The Netherlands, Sept. 2008.

[14] A. V. M. Ludovico, G. Vercellino and L. Accatino, "Multipaction analysis in high power antenna diplexers for satellite applications," in *Proceedings of the Workshop on Multipactor, RF and DC Corona and Passive Intermodulation in Space RF Hardware*, ESTEC, Noordwijk, The Netherlands, September 2000, p. 109.

[15] C. Bachiller, H. González, V. Esbert, A. Martinez, and J. Morro, "Efficient Technique for the Cascade Connection of Multiple Two-Port Scattering Matrices," *Microwave Theory and Techniques, IEEE Transactions on*, vol. 55, no. 9, pp. 1880–1886, 2007.

[16] D. Pozar, *Microwave Engineering*. New York: John Wiley & Sons Inc., 1998.

[17] J. Reiter and F. Arndt, "Rigorous analysis of arbitrarily shaped H-and E-plane discontinuities in rectangular waveguides by a full-wave boundary contour mode-matching method," *Microwave Theory and Techniques, IEEE Transactions on*, vol. 43, no. 4, pp. 796–801, 1995.

[18] C. Bachiller, H. Esteban, H. Mata, M. Valdés, V. Boria, Á. Belenguer, and J. Morro, "Hybrid Mode Matching Method for the Efficient Analysis of Metal and Dielectric Rods in H Plane Rectangular Waveguide Devices," *Microwave Theory and Techniques, IEEE Transactions on*, vol. 58, no. 12, pp. 3634–3644, 2010.

[19] C. Bachiller, "Métodos híbridos para el análisis y diseño eficiente de filtros avanzados para sistemas de comunicaciones espaciales," Ph.D. dissertation, Universitat Politècnica de València, 2010, http://riunet.upv.es/handle/10251/8657.

[20] D.Budimir, *Generalized Filter Design by Computer Optimization*. London: Artech House, 1998.

[21] J. V. Morro, P. Soto, H. Esteban, V. Boria, C. Bachiller, M. Taroncher, S. Cogollos, and B. Gimeno, "Fast automated design of waveguide filters using aggressive space mapping with a new segmentation strategy and a hybrid optimization algorithm," *IEEE Trans. Microwave Theory Tech.*, vol. 53, no. 4, pp. 1130–1142, April 2005.

[22] J. V. Morro, C. Bachiller, H. Esteban, and V. E. Boria, "New efficient and robust automated design strategy for H plane direct-coupled-cavities filters with dielectric resonators," in *Proc. of the 2006 AP-S Int. Symp., pp. 597-600*, Alburquerque, June 2006, pp. 597–600.

[23] "Multipactor calculator," http://multipactor.esa.int, accessed: 2015-05-14.

[24] F. Quesada, "Investigation of multipaction phenomena in cavity filters loaded with dielectric posts and tuning elements." *Mulcopim 05: 5th International Workshop on Multipactor, Corona and Passive Intermodulation in Space RF Hardware*, The Netherlands September 2005.

[25] C. Bachiller, H. Esteban, J. Morro, and V. Boria, "Hybrid mode matching method for the efficient analysis of rods in waveguide structures," *Mathematical and Computer Modelling*, vol. 57, no. 2013, pp. 1832–1839, 2013.

[26] "Pinach (alborache, valencia, spain)," http://www.pinach.com/, accessed: 2015-05-14.

[27] "Morgan advanced ceramics. material D20," http://www.morganadvancedmaterials.com/sites/default/files/documents/morgan_dielectric_br_web_18.02.15_singe_pages.pdf, accessed: 2015-09-15.

[28] O. Monerris Belda, E. Diaz Caballero, J. Ruiz Garnica, and V. Boria, "Automatic, calibrated and accurate measurement of S-parameters in climatic chamber," *Microwave and Wireless Components Letters, IEEE*, vol. 25, no. 6, pp. 412–414, June 2015.